PAPER

Check for updates

Designing novel anti-plasmodial quinoline–furanone hybrids: computational insights, synthesis, and biological evaluation targeting *Plasmodium falciparum* lactate dehydrogenase†

Deepika Choudhary, [ID] [a] Poonam Rani,[b] Naresh Kumar Rangra,[c] Girish Kumar Gupta, [ID] [d] Sukhbir Lal Khokra,*[e] Richie R. Bhandare [ID] *[fg] and Afzal B. Shaik [ID] *[h]

To combat resistance against current antimalarials, modifying key pharmacophores and exploring novel parasite-specific drug targets remained one of the key drug design strategies. The resistance to quinoline-based antimalarials arises often due to the efflux of the drug. Hence, the development of newer agents containing bulkier pharmacophores will enable medicinal chemists to counteract drug resistance. In view of this, herein we designed bulkier quinoline–furanone hybrids. Initially, virtual drug-likeness and ADMET screening were conducted to optimize physicochemical properties followed by docking of the hybrids against the *Plasmodium falciparum* lactate dehydrogenase (*Pf*LDH) enzyme. The most potent hybrids that emerged from the computational screening were synthesized and screened for their bioactivity against the resistant strain of *Plasmodium* through Schizont Maturation Inhibition assays. Among the compounds tested, **5g** and **6e** demonstrated the best activity, with IC$_{50}$ values similar to chloroquine (CQ), and **5g** exhibited superior LDH inhibition compared to CQ. Compounds **5f**, **7a**, and **7f** showed IC$_{50}$ values comparable to CQ and moderate LDH inhibition. Structure–activity relationship (SAR) analysis revealed that halogen substitutions, particularly Br and Cl, enhanced antimalarial activity, while strong electron-withdrawing (–NO$_2$) or -donating (–OH) groups led to diminished activity. Additionally, bulkier aromatic substitutions were favoured for antimalarial activity and LDH inhibition. The investigation successfully found potent anti-plasmodial quinoline–furanone hybrids, demonstrating promising prospects for combating malaria.

[a]Department of Pharmaceutical Sciences and Natural Products, Central University of Punjab, Bathinda-151401, Punjab, India. E-mail: ms_deepika86@yahoo.com

[b]Department of Pharmaceutical Sciences, Guru Jambheshwar University of Science and Technology, Hisar-125001, Haryana, India

[c]Chitkara School of Pharmacy, Chitkara University, Baddi, Himachal Pradesh, India. E-mail: nareshrangra@gmail.com

[d]Department of Pharmaceutical Chemistry, Sri Sai College of Pharmacy, Badhani, Pathankot-145001, Punjab, India

[e]Institute of Pharmaceutical Sciences, Kurukshetra University, Kurukshetra-136119, Haryana, India. E-mail: slkhokra@kuk.ac.in

[f]Department of Pharmaceutical Sciences, College of Pharmacy and Health Sciences, Ajman University, P. O. Box 346, Ajman, United Arab Emirates. E-mail: r. bhandareh@ajman.ac.ae

[g]Centre of Medical and Bio-allied Health Sciences Research, Ajman University, P. O. Box 346, Ajman, United Arab Emirates

[h]Center for Global Health Research, Saveetha Medical College, Saveetha Institute of Medical and Technical Sciences, India. E-mail: bashafoye@gmail.com

† Electronic supplementary information (ESI) available. See DOI: https://doi.org/10.1039/d4ra01804d

1. Introduction

Malaria is mainly a disease of parasitic infection which is considered to affect almost half of the world's population. As per the WHO, 247 million malaria cases and 0.619 million deaths were reported in the World Malaria Report 2022.[1] To combat this situation, the World Health Organization (WHO) recommended some preventive measures like vaccination for children and vector control.[2] Malaria has become one of the deadliest infections when caused by *P. falciparum* particularly in the case of children under 5 years. To reduce the risk of death in children living in malaria-endemic areas, the WHO recommended the use of the malaria vaccine RTS, S/AS01. Other than that the WHO also emphasizes the use of preventive chemotherapies and vector control. However, despite the various preventive measures the increasing resistance in plasmodium is worldwide, which in turn is a matter of concern for the WHO to meet the target of 2030 proposed for the malaria strategy. Furthermore, the current antimalarial drugs are associated with reduced effectiveness and resistance. Thus among the different

strategies, the search for new effective medicine as well as new drug targets should be given priority to combat malaria.[3]

Quinoline-based antimalarial drugs mainly chloroquine (CQ) have been used to treat infection and even complicated cases of malaria caused by *Plasmodium falciparum*. However as mentioned above, the major problem associated with CQ is resistance, making the drug ineffective.[4] One of the main reasons for the resistance and reduced effectiveness of the drug CQ is associated with the increased level of drug efflux from the receptor protein in plasmodium, as a result, resistant strains of parasite exhibit faster removal of the drug as compared to the chloroquine-sensitive parasites.[5] It has been reported that CQ efflux can be reduced by designing the bulkier molecules, as these were reported to be extruded with difficulty from the receptor protein.[6] The researchers have explored the potency of various bulky quinoline hybrids and found them effective even against resistant *P. falciparum* strains.[7] Another strategy that can play an important role in drug discovery and designing of new molecules is, hybridization and the use of computational tools, many hybrid compounds comprising of quinoline–triazole, quinoline–artemisinin, quinoline–chalcone, quinoline–pyrazole, quinoline–ferrocene and bis or tris quinoline (Fig. 1), *etc.* have also shown promising antimalarial activities in both drug-sensitive and resistant strains.[8–11]

The literature shows that even today the quinoline can be considered as the most versatile nucleus for the derivatization to get better potential antimalarial candidates. The concept of molecular hybridization and computational tools can further add benefits to the search for new drug targets and better chemotherapeutic agents for malaria. In consideration of all these points, various quinoline–furanone-based hybrids were designed (Fig. 2) and studied for their antimalarial potential against the resistant strain of *P. falciparum*. In context to explore the new drug target, Pf lactate dehydrogenase (*Pf*LDH) was selected as the target protein. Because *Pf*LDH is different from human LDH structurally,[12] therefore, the new compounds will be more specific for the parasite. The binding affinity of the designed ligands with the receptor has been evaluated by molecular docking using the 3D crystalline structure of the enzyme *Pf*LDH. The results were further confirmed by *in vitro* LDH assay. Furthermore, as we are designing some bulkier molecules, it is essential to screen them for their physio-chemical or drug-likeness properties, therefore their ADME-T profile was also accessed virtually using *in silico* tools.

2. Results and discussions

2.1 Chemistry and synthesis

*Pf*LDH can serve as a potential drug target for the drug discovery of new and effective antiplasmodial agents. Furthermore, the amalgamation of two different pharmacophores in one molecule and the use of computational tools to optimize the designed library of compounds can be a useful strategy in the search for new antiplasmodials.[12–17] With the use of some
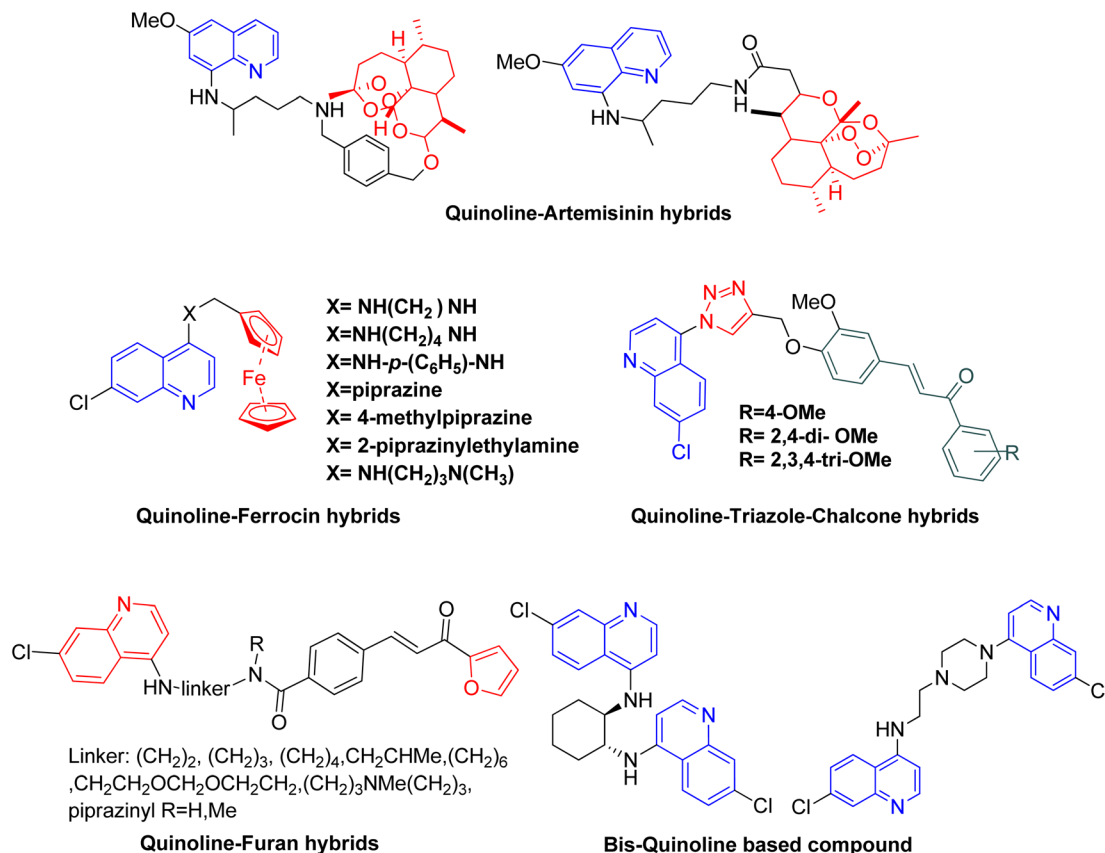

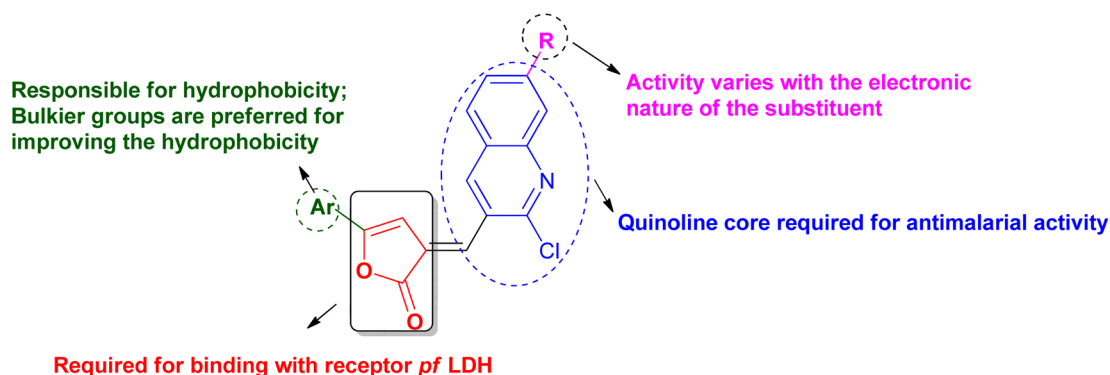**Fig. 1** Quinoline based hybrids as antimalarial agent.

Fig. 2 Drug design and SAR of quinoline–furanone hybrids.

important computational tools, strategies, and the reported SAR and available literature, libraries of furanone–quinoline hybrid ligands were generated.[18–20] This library was screened for its ADME-Toxicity profile and molecular docking. The 3D crystalline structure of *Pf*LDH was used as a target protein to screen the best hits. The whole virtual screening process with *in silico* ADME-T prediction and molecular docking, helped us to screen out the 11 best ligands from the library of a total of 24 designed hybrids. The synthetic scheme to prepare the best potent targeted compounds based on quinoline–furanone hybrids has been illustrated in Synthetic Scheme 1. The general structure of

designed derivatives and the physical data of the synthesized compounds have been represented in Tables 1 and 2 respectively.

The synthetic methodology was the same as the previously reported procedure,[9,10] however, we have utilized some different aryl group-based β-benzoyl propionic acid. The overall synthetic scheme involves three different steps (1) the synthesis of β-benzoyl propionic acid (2) the synthesis of quinoline-3-carbaldehyde derivatives (3) the condensation of quinoline-3-carbaldehyde with β-aroyl propionic acid to yield the target compounds. The Friedel–Crafts acylation was done in the
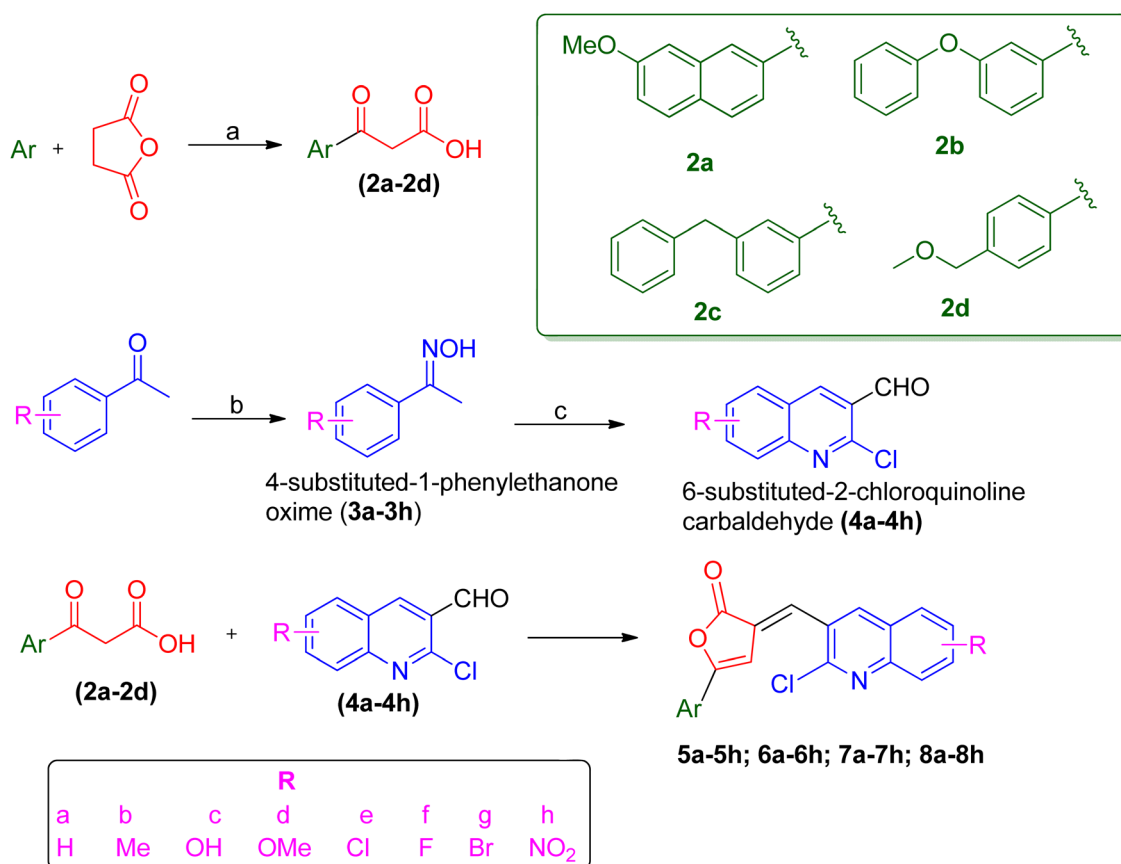
Scheme 1 *Reagents and conditions*: (a) anhydrous AlCl₃, reflux, 2–4 h (b) NH₂OH·HCl, CH₃COONa, ethanol, water, reflux for 1 h at 100 °C (c) DMF, POCl₃ stirring for 16 h at 50–60 °C at anhydrous condition (d) acetic anhydride, triethylamine, heat, 5 min, anhydrous condition.

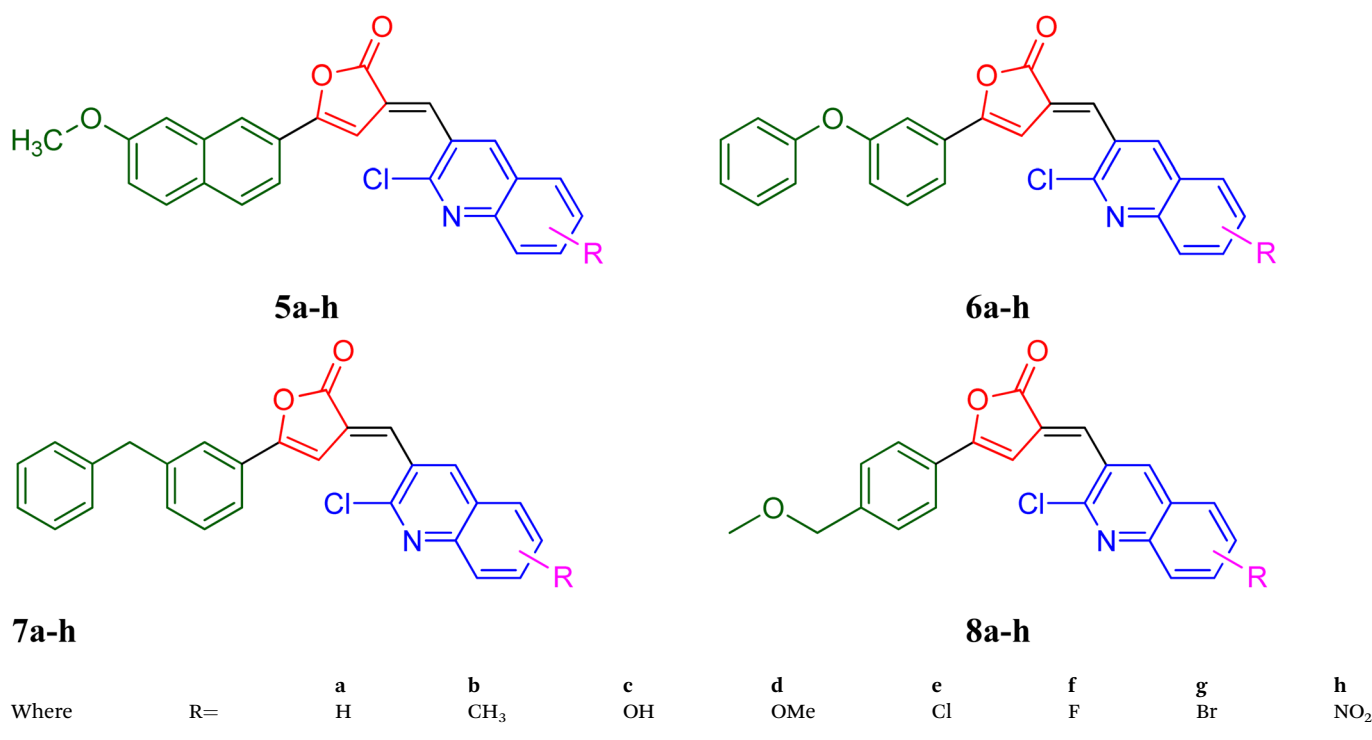**Table 1** General structures of designed quinoline–furanone hybrids

Where	R=	**a**	**b**	**c**	**d**	**e**	**f**	**g**	**h**
		H	CH$_3$	OH	OMe	Cl	F	Br	NO$_2$

Table 2 Physical data of synthesized furanone-bearing quinoline moieties

S. no.	Compound	R_f value	Melting point (°C)	Yield (%)
1	**5e**	0.88	245–246	42
2	**5f**	0.88	263–265	37
3	**5g**	0.79	172–174	22
4	**6a**	0.81	216–218	78
5	**6c**	0.87	248–250	85
6	**6e**	0.82	215–218	68
7	**6f**	0.83	235–238	42
8	**6h**	0.84	286–288	84
9	**7a**	0.86	110–112	73
10	**7f**	0.76	150–152	76
11	**7h**	0.71	184–186	28

presence of anhydrous aluminum chloride as a catalyst using 4 types of aromatic groups. The different substituted quinoline-3-carbaldehyde were prepared by Vilsmeier–Haack formylation using *N*,*N*-dimethylformamide (DMF) and phosphorus oxychloride (POCl$_3$) with a different acetophenone oxime.[21] Then the condensation of β-aroyl propionic acid with quinoline-3-carbaldehyde in the presence of acetic anhydride and triethylamine gives us the proposed compounds. The characterization of synthesized compounds is done by spectral techniques such as mass, FT-IR, ^{1}H-NMR, and elemental analysis. The IR spectral data of synthesized titled quinoline–furanone hybrids shows the characteristic bands of lactone at 1762–1687 (lactone, C=O) along with other bands corresponding to values like 1220–1136 (C–N), 1522–1435 (C=C) and 1567–1549 (C=N). The

peak in ^{1}H NMR spectra at δ value 6.5–7.5 confirm the cyclization to form furan ring. The presence of an alkene proton in place of an aldehydic proton also confirm the formation of the targeted compound.

2.2 Anti-malarial activity

Evaluation of antiplasmodial activity was done with all the synthesized derivatives by *in vitro* methods using chloroquine-resistant (K1) strains of *P. falciparum* procured from the Parasite Bank of the National Institute of Malaria Research (NIMR), New Delhi. The estimation of antiplasmodial activity was also carried out in the laboratory of the same institute. The standardized WHO Schizont Maturation Test (micro-test) and the colorimetric method mainly for parasite Lactate dehydrogenase inhibition (pLDH) were employed in the current studies for the estimation of the antiplasmodial potential of synthesized hybrid compounds. In the SMI assay, a thin smear from each well was prepared according to the reported method[22] and as the parameter of antiplasmodial activity assessment was the number of schizonts, the compounds in which a lesser number of mature schizonts appear in comparison with control well, were considered active as they affect the formation of schizont from ring stage. As a consequence, it was reported that the greater the number of mature schizonts, the lesser will be the %inhibition of parasitemia, hence very low activity. The images of the microscopic view of parasitized erythrocytes of culture from standard as well as test compounds are shown below in Fig. 3A–D.

On the other hand in the pLDH assay, the measurement of activity of pLDH activity was the criteria, which in turn depends
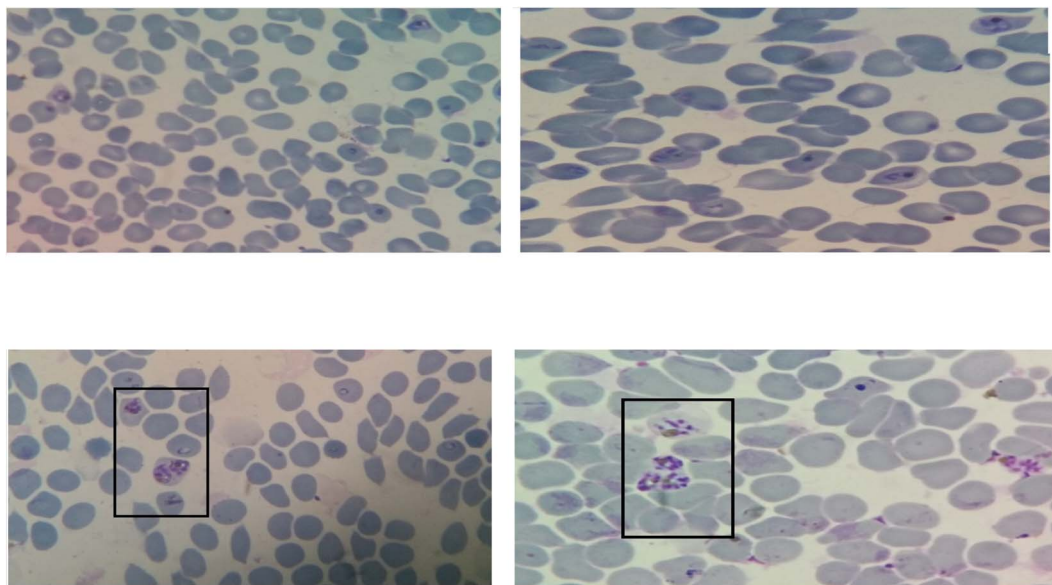

—

Fig. 3 (A) The microscopic view of parasitized erythrocytes from culture having standard drug, reported with no mature schizont. (B) The microscopic view of parasitized erythrocytes from the culture of the potent test compound, reported only with some early schizont, but no mature schizont appear. (C) The microscopic view of parasitized erythrocytes from the culture of the moderately potent compound, reported with a few no. of mature schizonts (shown inside the black rectangle). (D) The microscopic view of parasitized erythrocytes from the culture of less active compound, having comparatively more number of mature dividing schizonts (shown inside the black rectangle).

on the value of absorbance given by the plate reader.[23] During this assay, it was observed that the enzymatic activity detected in infected erythrocytes from the control well was at least twice that of standard CQ. Moreover, the value of absorbance given by the control well was considered as 100% pLDH activity. Therefore based on the above specifications the value of absorbance for the test compounds was analyzed and results revealed that as the drug concentration increased, the corresponding value of absorbance was decreasing. The corresponding IC_{50} was calculated from the number of schizonts in SMI and the value of absorbance in pLDH. The potency criteria referred in both methods was based on the WHO criteria such as the compounds, those having IC50 value ≥ 10 exhibited poor antiplasmodial activity, those having IC50 value ≥ 5 were considered to possess moderate antiplasmodial activity, while the compounds having IC_{50} value less than 5 were considered the most active compounds among all. The data for the in vitro test is shown in Table 3.

The in vitro antiplasmodial activity data depicted that the compounds 5g and 6e were exhibiting maximum activity with IC_{50} value almost similar to the CQ. A total of 6 compounds 5e, 5f, 6a, 6f, 7a, and 7f, showed IC_{50} values comparable to CQ (<5) and after them, the compound 7h was found comparatively less potent, and the other two compounds 6c and 6h were found to have very poor antiplasmodial potential with IC_{50} >10 as shown in Table 3. The results of in vitro activity data give some important information regarding SAR of designed derivatives such as derivatives with either H or halogen as R will lead to an increase in antiplasmodial activity but substitution either with the strong electronic withdrawing group like $-NO_2$ or strong electronic donating group like OH, result in almost loss or very less activity. The overall observation from in vitro

Table 3 The inhibitory concentrations value (IC values in $\mu g\ mL^{-1}$) of quinoline–furanone based on in vitro antiplasmodial activity

Compound	Antiplasmodial activity by SMI method			Antiplasmodial activity by PfLDH inhibition method		
	IC_{50}	IC_{90}	IC_{99}	IC_{50}	IC_{90}	IC_{99}
5e	3.251	24.143	66.153	4.283	24.431	122.192
5f	2.825	15.125	54.156	3.014	12.474	28.163
5g	2.083	7.794	32.114	2.314	12.162	23.118
6a	3.125	16.425	105.134	6.567	79.142	179.784
6c	23.792	382.468	453.024	16.710	276.112	295.828
6e	2.168	5.952	25.112	4.738	16.129	23.061
6f	3.960	27.479	124.499	5.379	77.479	128.428
6h	16.837	252.719	312.148	14.294	216.952	228.113
7a	2.473	18.129	39.115	3.202	12.836	18.184
7f	2.569	12.129	28.591	5.393	17.425	22.402
7h	8.216	67.126	125.362	5.539	88.586	203.628
CQ (standard)	1.953	2.118	9.862	2.873	3.102	10.046

antiplasmodial analysis concluded that both the quinoline and furanone can be considered important pharmacophores to design newer antiplasmodial agents which may have act as inhibitors of specific targets such as PfLDH.

2.3 Computational studies

In the process of rational drug discovery, the toxicity and bad pharmacokinetics (ADME-T) profiles are the main reason behind the failure of drugs at the later stages of drug development.[24] The in silico methods like prediction of ADME-T and study of binding interaction of ligands within the protein receptor by molecular docking studies play very crucial roles in

the optimization of designed hits and can reduce the overall cost as well as time of drug discovery.[25] The virtual screening and insilico analysis of the designed derivatives using computational tools like QikProp for ADME prediction, TOPKAT for toxicity studies, and Molegro Virtual Docker (MVD) for molecular docking are discussed here.

2.3.1 ADME-T prediction. A total of 11 hits from 24 designed ligands were screened as "non-toxic, drug-like molecules" on the basis of different parameters given in the software TOPKAT and QIKProp. 3.6. ADME filter and Toxicity prediction analysis revealed that the filtered hits lay in the optimum range. The values of different descriptors used for ADME prediction are shown in Table 4. The range for important parameters was predicted such as value of molecular weight lay in the range between 423 to 527, total solvent accessible surface area (SASA) ranged from 725 to 868, the number of hydrogen bonds donor (Donor HB) was between 0.0 and 1.0, the estimated number of hydrogen bonds acceptor was ranged between 3 and 8 predicted octanol/gas partition coefficient (QP log Poct) ranged 18–25, predicted water/gas partition coefficient (QP log Pw) ranged 8–17, predicted octanol/water partition coefficient (QP log Po/w) ranged 5–7, predicted aqueous solubility, log S (QP log S) ranged −9 to 4, predicted brain/blood partition coefficient (QP log BB) ranged −1.5 to −0.8, and Lipinski violations were ≤1. Toxicity prediction was done by TOPKAT, in this prediction the designed library was screened for carcinogenicity and mutagenicity filter in rat model, and the results are represented in Table 5. The predictions in TOPKAT were performed through a search program based on similarity along with a check that weather the test structure prediction lies in the optimum prediction space (OPS) or not. The OPS also permits the user to determine if structures are within the model descriptor space, but in some cases, the toxicity can be predicted of those compounds that lie outside OPS. This current analysis revealed that the 11 screened analogs may have good ADME-T properties and can be successful drugs in the future.

2.3.2 Molecular docking. The hits screened from the ADME-T filter, were then subjected to molecular docking analysis, to study their binding interaction with the receptor protein *i.e.* *Pf*LDH. The binding mode and the requisite interactions with specific amino acids were compared with the internal ligands and the standard drug CQ using the software MVD as given below.

2.3.2.1 Prediction of the binding site. The 3D crystalline structure of receptor protein *Pf*LDH having with NADH and the substrate Oxamate (co-crystalized ligands of 1LDG) was imported from the Protein Data Bank (https://www.rcsb.org) (Fig. 4) into the workspace of the software and different steps of protein preparation were done which include the deselection of all water molecules having specific distance more than 5 Å, selection of suitable cavity, or binding site prediction in *Pf*LDH receptor. The search algorithm in MVD showed a total of five cavities of different volumes in protein. It was observed that NADH, Oxamate, and CQ were going in Cavity-1, with the

Table 5 Toxicity prediction of best hits shown by TOPKAT[a]

Compound	ops1	ops2	Fragment	Carcinogenicity	Mutagenicity
5e	TRUE	TRUE	TRUE	0.316	X
5f	TRUE	TRUE	TRUE	0.368	X
5g	TRUE	TRUE	TRUE	0.374	X
6a	TRUE	TRUE	TRUE	0.011	X
6c	TRUE	TRUE	TRUE	0.012	X
6e	TRUE	TRUE	TRUE	0.019	X
6h	TRUE	TRUE	TRUE	0.023	X
6f	TRUE	TRUE	TRUE	0.024	X
7a	TRUE	TRUE	TRUE	0.241	X
7f	TRUE	TRUE	TRUE	0.006	X
7h	TRUE	TRUE	TRUE	0.009	X

[a] Toxicity descriptors calculated from TOPKAT. Ops1 and Ops2 – optimum prediction state.

Table 4 ADME-T prediction data for the filtered "druglike" hits[a]

Compound	MW	SASA	HBD	HBA	Qp log Po/w	QP log S	QP log Khsa	%HOA	PSA	AffyMDCK	Affy Caco-2	Qp log BB	QP log Poct	QP log PW	Rule of 5
5e	448.301	738.215	0	4	6.67	−6.534	1.038	100	52.34	2832.427	2437.056	−0.426	22.741	11.472	1
5f	431.842	759.438	0	4	5.18	−6.287	1.283	100	52.34	2743.324	2463.728	−1.257	24.042	11.037	1
5g	492.752	749.358	0	4	6.80	−7.539	1.047	100	52.34	2853.320	2353.132	−0.238	24.846	12.571	1
6a	425.87	725.503	0	4	6.157	−7.463	1.097	100	56.75	2627.307	2441.144	−0.232	18.752	8.954	0
6c	439.897	757.677	0	4	6.483	−8.073	1.27	100	56.749	2628.822	2442.458	−0.25	19.26	8.651	0
6e	441.87	737.753	1	4.75	5.498	−7.382	1.014	100	79.283	7242.81	7412.54	−0.894	20.937	11.05	1
6h	460.315	749.448	0	4	6.662	−8.229	1.225	100	56.752	6484.175	2441.959	−0.07	19.446	8.713	1
6f	443.861	734.438	0	4	6.397	−7.838	1.143	100	56.753	4715.541	2441.398	−0.122	19.006	8.733	1
7a	470.868	763.748	0	5	5.404	−7.502	0.998	89.77	101.629	2651.75	2932.023	−1.391	21.195	10.07	0
7f	423.898	736.238	0	3.5	8.292	−7.929	1.32	100	48.904	2627.1	2440.781	−0.231	18.88	8.292	1
7h	437.92	767.937	0	3.5	6.891	−8.53	1.493	100	48.903	2628.787	2442.182	−0.248	19.383	7.984	1

[a] The descriptor was calculated from QIKProp 3.6. where each descriptor represent one physicochemical property for "drug likeliness" such as MW – molecular weight; SASA – solvent assessable surface area; HBD – no. of H bond donor; HBA – no. of H bond acceptor; QP log Po/w – predicted octanol/water partition coefficient; QP log S – predicted aqueous solubility; QP log Khsa – predicted human serum albumin binding; %HOA – percentage human oral absorption; PSA – total polar surface area; AffyMDCK – predicted apparent MDCK cell permeability in nm s^{-1}, Affy Caco-2 – predicted apparent Caco-2 cell permeability in nm s^{-1}, Qp log BB – predicted blood–brain partition coefficient, QP log Poct – predicted octanol/gas partition coefficient, QP log PW – predicted water/gas partition coefficient rule of 5-Lipinski violations.
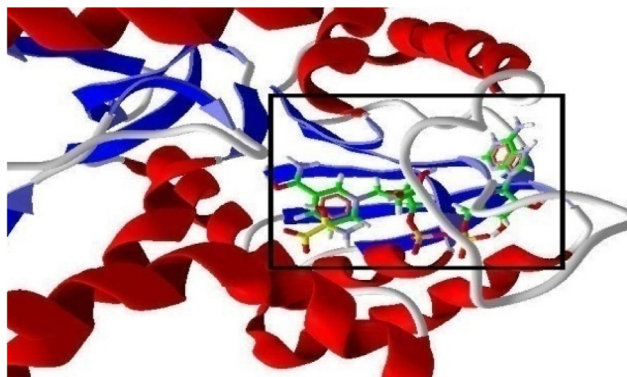
Fig. 4 3D structure of the protein (1LDG) showing binding of NADH and Oxamate (highlighted in a window) within the pocket of *Pf*LDH.

largest volume and size, approximately 136.096 Å. Therefore this particular cavity was selected and others were rejected.

2.3.2.2 Binding mode analysis. Two major binding sites were predicted on the target protein (1LDG). One of which was the NADH binding site and another was the substrate binding domain.[26] NADH binding site was identified on the N-terminal end of the enzyme with Gly 29, Ile31, Asp53, Ile54, Thr97, Gly99, Phe100, and Asn140 as key amino acids. The adenine end of the cofactor side of the binding pocket is formed by these amino acid residues and goes deep into the protein towards the nicotinamide end of the cofactor site, the substrate binding domain or the second site was constituted by amino acid residues on the C-terminal end of enzymes such as Arg109, Asn140, Arg171, His195, Val233, Ala236 and Ser245. The amino acid residues formed a binding groove on the back side of the substrate active site lying approximately 10 Å deep within the protein structure, adjacent to the nicotinamide end of the cofactor site. All the filtered hits were successfully docked to the receptor *Pf*LDH. After the visual binding mode analysis of the standard drug CQ, the bound ligand NADH and other ADME-T filtered hits, it was observed that all the screened hits (quinoline–furanone hybrids) were exhibited binding within the same cavity along with NADH and CQ. Moreover, it was also revealed that the screened designed hybrids not only showed better mol dock scores but having optimum interactions with the specific amino acid residues including Gly 29, Ile31, Asp53, Ile33, Thr97, Gly99, Phe100, Asn140, Arg171, His195, and Ser245. Along with that, their binding conformations were well superimposed with NADH (Fig. 5A). Molecular docking analysis concluded that these hits may exhibit competitive inhibition with of NADH which is considered essential for the enzyme *Pf*LDH.

2.3.2.3 Calculation of binding energy and docking scores. The molecular docking data revealed that all the nontoxic druglike, compounds **5e–g**, **6a**, **6c**, **6e**, **6f**, **6h**, **7a**, **7f** and **7h** exhibited comparative to good binding score with strong H-bond interaction with the receptor *Pf*LDH, as represented in Table 6. The compounds **6c**, **6e**, **6h**, **7a**, and **7h** showed the best moldock score with maximum binding energy, best binding conformation, and good interactions within the receptor. All ligands have good moldock score which was more than −100 except **6a** and **7f** in MVD (Table 6). Besides, it was also found that each ligand's
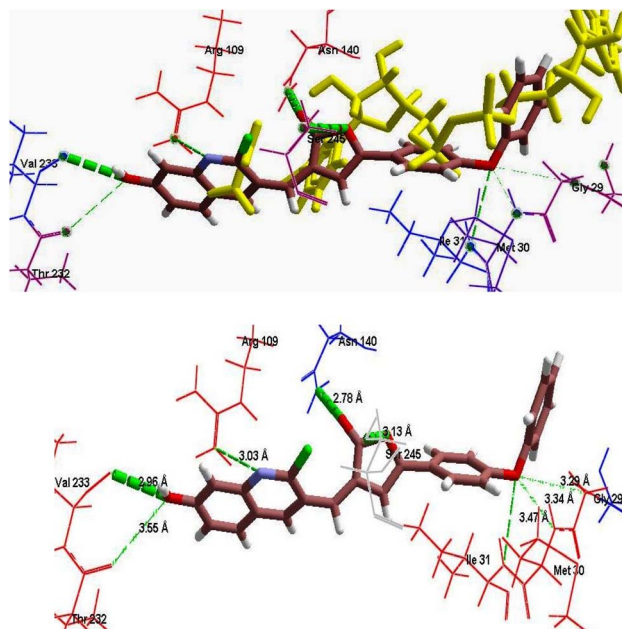

Fig. 5 (A) Superimposition in the binding mode of **6c** (dark pink) with NADH, (shown in yellow color) in the pocket of protein receptor *Pf*LDH (1LDG). (B) The binding mode of compound **6c** in the pocket of protein receptor *Pf*LDH (1LDG), having H-bond Interactions (green dotted lines) with the key amino acids.

Table 6 Docking results of best-screened compounds for *Pf*LDH inhibition on Molegro

S. no.	Ligands	Moldock score	Interacting residues and H-bond interaction with distance (Å)
1	**NADH**	−217.75	Asn140 (2.65), Asn140 (3.42), Asn140 (3.13), Gly99 (3.20), Thr97 (3.38), Thr97 (2.17), Arg109 (3.09), Arg109 (2.67), Ile31 (3.13), Ser245 (2.75), Pro246 (2.41), Phe100 (2.99), Thr139 (3.25), Arg116 (3.02)
2	**CQ**	−153.55	Ser245 (3.21), Asn140 (2.99)
3	**5e**	−120.36	Arg109 (2.64), Asn140 (3.36), Ser245 (3.28)
4	**5f**	−114.52	His195 (3.62), Asn140 (3.47), Arg109 (2.81)
5	**5g**	−106.37	Ala236 (3.61), Gly29 (3.74)
6	**6a**	−99.23	Gly29 (3.03), Ser245 (2.73), Asn140 (3.01)
7	**6c**	−122.07	Arg109 (3.03), Asn140 (2.78), Ser245 (3.13), Met30 (3.34), Gly29 (3.29), Ile31 (3.47), Val233 (2.96), Thr232 (3.55)
8	**6e**	−122.57	Ser245 (2.87), Asn140 (2.97), Gly29 (3.02)
9	**6f**	−119.09	Ala236 (3.07), Arg109 (2.84), Asn140 (3.12)
10	**6h**	−132.77	Arg109 (2.46), Arg171 (2.72), Arg171 (2.38), Ala236 (3.45), Gly29 (3.27), Ser245 (3.29), Asn140 (3.12), Ser28 (3.33)
11	**7a**	−148.01	Asn140 (2.97), Ser245 (3.33)
12	**7f**	−97.723	Ser245 (3.38), Asn140 (2.96), Arg109 (3.13)
13	**7h**	−150.98	Ala236 (3.17), Arg171 (2.58)

binding pose was much closer to NADH and CQ with good superimposition (Fig. 4–6). It was observed that each filtered hit made consistent hydrogen bond interactions with the key amino acids such as Met30, Ile31, Asp53, Gly99, Try85, Arg109, Asn140, Arg171, Ser245, Ala236, and Thr232, which were the same as in case of the binding of reported *Pf*LDH inhibitors. The results elucidated that CQ as well as screened hits may have a similar inhibitory mechanism against enzyme *Pf*LDH as they can act as competitive inhibitors of NADH for binding within the receptor protein.

3. Material and methods

The compounds were synthesized using commercially available analytical grade chemicals without purification from E. Merck (Germany) and S. D. Fine Chem. Lmt (India). Melting points
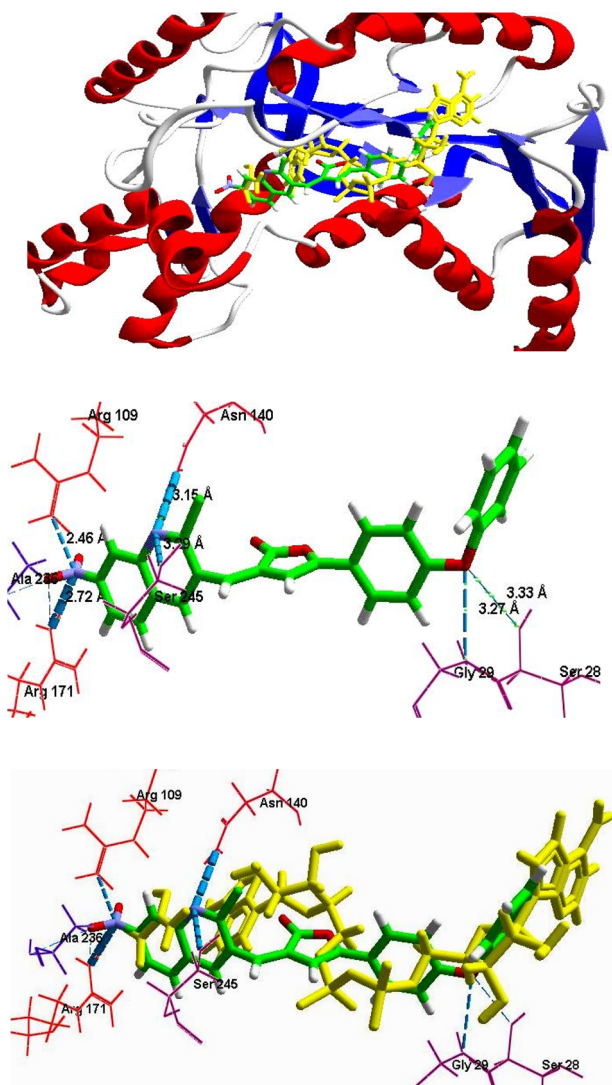

Fig. 6 (A) Binding mode of **6h** (green color) with NADH and substrate Oxamate (shown in yellow color) in the pocket of protein receptor *Pf*LDH (1LDG). (B) Binding mode of **6h** in the pocket of protein receptor *Pf*LDH, having H-bond interaction with key amino acids. (C) Superimposition in the binding mode of **6h** (green) with NADH (shown in yellow color) in the pocket of protein receptor *Pf*LDH (1LDG).

(MPs) were taken on slides using Labindia electrical visual melting range apparatus and are uncorrected. Benzoic acid was used as reference for the calibration of melting point apparatus. IR spectra were recorded on a PerkinElmer 1800 FT-IR spectrophotometer. ^{1}H NMR spectra were recorded on a Bruker 300 & 400 MHz instrument using tetramethylsilane as an internal standard. Mass spectra were recorded on 2500 eV (ESI Source) using a water's Q-TOF microinstrument and elemental analysis on the PerkinElmer 2400 instrument. Progress of the chemical reaction and the purity of the synthesized compound were checked on silica gel G-coated thin-layer chromatography plates in solvent systems; petroleum ether : toluene : ethyl acetate (5 : 4 : 1, v/v/v). The visualization of spots on TLC was carried out in either in an iodine chamber or in UV cabinet at a long wavelength under a UV lamp.

3.1 Chemical synthesis of virtually screened ligands

The whole synthetic scheme was done in the following steps.

3.1.1 Synthesis of succinic anhydride (1). Succinic acid (0.1 mol) was taken in sufficient volume of acetic anhydride in a round bottom flask. The reaction mixture was refluxed using a water bath with occasional shaking until a clear solution was obtained. Refluxing was continued for a further hour to ensure the completion of the reaction. The reaction mixture was cooled to room temperature to get crystals of succinic anhydride. After that washing of crystals was done three times with anhydrous ether and dried in vacuum desiccators. The melting point of the compound was determined.

3.1.2 Synthesis of β-aroylpropionicacids (2a–d)

3.1.2.1 Synthesis of 3-(7-methoxy-2-naphthoyl) propionic acid (2a). Dry nitrobenzene was added to the mixture of succinic anhydride (0.1 mol) and 2-methoxy-naphthalene (0.1 mol) in a round bottom flask. The mixture was heated with stirring to dissolve the content and then cooled to room temperature. Anhydrous aluminum chloride was added to a well-stirred mixture over 20 minutes, and the stirring was continued for 2–3 hours under anhydrous conditions. The reaction was allowed to stand for 2 days at room temperature while maintaining an anhydrous condition. The completion of the reaction was checked from time to time using TLC. After that excess nitrobenzene was evaporated under vacuum at 110–140 °C. A 10% sodium hydroxide solution was added to dissolve the desired reaction product and filtered to remove undissolved and unwanted material. The above solution was neutralized by the addition of dilute hydrochloric acid. Finally, precipitates of aroylpropionic acid were filtered and washed with cold water, and recrystallized with ethanol. The melting point of the compound was determined.

Note: Nitrobenzene was dried by adding 20 g anhydrous magnesium sulfate in 250 ml nitrobenzene and kept overnight.

3.1.2.2 General procedure for the synthesis of 3-(3-phenoxy-2-phenoyl)propionic acid; 2b, 3-(3-benzyl-2-phenoyl)propionic acid; 2c and 3-(2-(methoxymethyl)-1-phenoyl)propionic acid; 2d. Succinic anhydride (0.1 mol) was dissolved in 50 ml of dried starting material (diphenyl ether for **2b**, diphenylmethane for **2c**, and methoxy methyl benzene for **2d**) under the anhydrous

condition in the presence of anhydrous aluminum chloride (0.2 mol). The reaction mixture was refluxed for 2–4 hours. The reaction product was purified by dissolving in sodium hydroxide solution and filtered to remove undissolved and unwanted material. The above solution was neutralized by the addition of dilute hydrochloric acid. Finally, precipitates of aroylpropionic acid were filtered and washed with cold water, and recrystallized with ethanol. The melting point of the compound was determined.

3.1.3 General procedure for the synthesis of 4-substituted-1-phenylethanone oximes (3a–h). To the solution of acetophenone (0.1 mol) in ethanol, hydroxylamine hydrochloride (0.1 mol) was added. To the above mixture, sodium acetate (0.12 mol) and a sufficient amount of water was added to dissolve it. Then the reaction mixture was refluxed on water bath for 3 to 6 hours. The monitoring and completion of the reaction was done using TLC. After completion of the reaction, the mixture was cooled, the product was precipitated out. The precipitated product was filtered and recrystallized with ethanol and finally the melting point of the compound was determined.

3.1.4 Synthesis of substituted-2-chloroqinoline-3-carbaldehydes (4a–h). Dimethylformaldehyde (0.15 mol) cooled to 0 °C, and to this freshly distilled phosphorusoxychloride (0.35 mol) was added dropwise under stirring in a ice bath, then the respective oxime (0.05 mol) was added portionwise. After the addition the reaction mixture was stirred at 50–60 °C for 16 h. It was then poured into ice water (300 ml) and stirred at 0 to 10 °C for 30 min. The 2-chloroquinoline-3-carbaldehyde was filtered and recrystallized with ethyl acetate.

3.1.5 General procedure for the synthesis of 3-{(2-chloro-6-substituted-quinolin-3-yl)methylene}-5-(aryl-2-yl)-furan-2(3H)-one (5e–g, 6a, 6c, 6e, 6f, 6h, 7a, 7f and 7h). To equimolar quantity (0.005 mol) of aroyl propionic acid (2a–d) and aromatic aldehyde (4a–h), we added acetic anhydride to wet the reaction mixture after that two–three drops of triethylamine were also added as a base. Then reaction mixture was heated for 5 minutes to fuse the mixture. After completion of the reaction, the content was poured into crushed ice in a small portion while stirring. A colored solid mass so separated was filtered and washed with cold water, then dried which on re-crystallization from methanol gave the desired compound. The melting point of the compound was determined.

3.1.5.1 (3-(2,6-Dichloroquinolin-3-yl)methylene)-5-(7-methoxynaphthalen-2-yl)furan-2(3H)-one 5e. Yield 42%; m.p. 245–246 °C: brown colour, R_f 0.88, IR(KBr) cm^{-1}: 1767 (C=O), 1560 (C=N str), 1203 (C–N str), 1497 (C=C str), ^{1}H NMR (300 MHz, CDCl$_3$): 6.81 (s, 1H, βH), 7.28 (s, 1H, olefinic H), 7.45–8.18 (complex m, 11H, arylprotons). ^{13}C NMR (100 MHz, CDCl$_3$) δ/ppm: 167.4 (1C, C-2), 148.4 (1C, C-3), 136.3 (1C, C-5), 125.9 (1C, CH, C-4), 98.4 (1C, CH, ethylene), 131.4 (1C, C'-naphthelene), 127.2 (1C, C', CH-naphthelene), 139.2 (1C, C'-naphthelene), 129.4 (1C, C'-naphthelene), 124.2 (1C, C', CH-naphthelene), 119.7 (1C, C'-CH-naphthelene), 105.3 (1C, C', CH-naphthelene), 158.2 (1C, C'-naphthelene), 118.5 (1C, C'-CH-naphthelene), 126.3 (1C, C', CH-naphthelene), 55.9 (1C, CH$_3$), 130.5 (1C, C-quinoline), 135.6 (1C, CH-quinoline), 126.4 (1C, C-quinoline), 128.4 (1C, CH-quinoline), 127.4 (1C, CH-quinoline), 130.8 (1C, -CH-

quinoline), 127.5 (1C, CH-quinoline), 147.0 (1C, C-quinoline), 149.5 (1C, C-quinoline), MS: m/z: 449 (M$^+$, 100%). Anal. calcd for C$_{25}$H$_{15}$Cl$_2$NO$_3$: C, 66.98; H, 3.37; N, 3.12; found: C, 67.28; H, 3.11; N, 3.52.

3.1.5.2 (3-(2-Chloro-6-fluoroquinolin-3-yl)methylene)-5-(7-methoxynaphthalen-2-yl)furan-2(3H)-one 5f. Yield 37%; m.p. 263–265 °C, yellow colour, R_f 0.88, IR (KBr) cm^{-1}: 1758 (C=O), 1556 (C=N str), 1210 (C–N str), 1428 (C=C str), ^{1}H NMR (300 MHz, CDCl$_3$): 6.72 (s, 1H, βH), 7.47 (s, 1H, olefinic H), 4.28 (s, 3H, OCH$_3$), 7.53 (d, 2H, ArH), 7.12 (d, 1H, ArH), 7.18 (d, 1H, ArH), 6.82 (d, 1H, ArH), 6.41 (d, 1H, ArH), 8.23 (s, 1H, quinoline-H), 7.59 (s, 1H, quinoline-H), 7.50 (d, 1H, quinoline-H), 8.42 (d, 1H, quinoline-H), ^{13}C NMR (100 MHz, CDCl$_3$) δ/ppm: 52.7 (1C, CH$_3$), 133.2 (1C, C-quinoline), 134.7 (1C, CH-quinoline), 127.7 (1C, C-quinoline), 125.2 (1C, CH-quinoline), 126.8 (1C, CH-quinoline), 131.6 (1C, -CH-quinoline), 128.7 (1C, CH-quinoline), 148.3 (1C, C-quinoline), 149.2 (1C, C-quinoline), 168.3 (1C, C-2), 142.7 (1C, C-3), 135.2 (1C, C-5), 127.9 (1C, CH, C-4), 97.8 (1C, CH, ethylene), 130.3 (1C, C'-naphthelene), 125.8 (1C, C', CH-naphthelene), 137.9 (1C, C'-naphthelene), 122.3 (1C, C'-naphthelene), 129.3 (1C, C', CH-naphthelene), 118.2 (1C, C'-CH-naphthelene), 107.5 (1C, C', CH-naphthelene), 157.4 (1C, C'-naphthelene), 115.2 (1C, C'-CH-naphthelene), 123.8 (1C, C', CH-naphthelene), MS: m/z: 432 (M$^+$, 100%). Anal. calcd for C$_{25}$H$_{15}$ClFNO$_3$: C, 69.53; H, 3.50; N, 3.24; found: C, 68.98; H, 3.27; N, 3.49.

3.1.5.3 (3-(6-Bromo-2-chloroquinolin-3-yl)methylene)-5-(7-methoxynaphthalen-2-yl)furan-2(3H)-one; 5g. Yield 22%; m.p. 172–174 °C: light pink colour, R_f 0.79, IR (KBr) cm^{-1}: 1688 (C=O), 1564 (C=N str), 1190 (C–N str), 1489 (C=C str), ^{1}H NMR (300 MHz, CDCl$_3$): 6.88 (s, 1H, βH), 7.58 (s, 1H, olefinic H), 4.12 (s, 3H, OCH$_3$), 7.45 (d, 2H, ArH), 7.08 (d, 1H, ArH), 7.23 (d, 1H, ArH), 6.79 (d, 1H, ArH), 6.46 (d, 1H, ArH), 8.13 (s, 1H, quinoline-H), 7.85 (s, 1H, quinoline-H), 7.52 (d, 1H, quinoline-H), 8.37 (d, 1H, quinoline-H), ^{13}C NMR (100 MHz, CDCl$_3$) δ/ppm: 161.8 (1C, C-2), 140.5 (1C, C-3), 126.6 (1C, CH, C-4), 136.4 (1C, C-5), 98.9 (1C, CH, ethylene), 134.3 (1C, C'-naphthelene), 138.3 (1C, C'-naphthelene), 128.6 (1C, C'-naphthelene), 124.9 (1C, C', CH-naphthelene), 123.6 (1C, C', CH-naphthelene), 119.7 (1C, C'-CH-naphthelene), 115.2 (1C, C', CH-naphthelene), 155.9 (1C, C'-naphthelene), 127.2 (1C, C', CH-naphthelene), 114.8 (1C, C'-CH-naphthelene), 56.8 (1C, CH$_3$), 134.1 (1C, C-quinoline), 135.8 (1C, CH-quinoline), 128.5 (1C, C-quinoline), 126.7 (1C, CH-quinoline), 127.4 (1C, CH-quinoline), 130.6 (1C, -CH-quinoline), 127.3 (1C, CH-quinoline), 144.9 (1C, C-quinoline), 147.4 (1C, C-quinoline), MS: m/z: 493 (M$^+$, 100%). Anal. calcd for C$_{25}$H$_{15}$BrClNO$_3$: C, 60.94; H, 3.07; N, 2.84; found: C, 60.59; H, 3.02; N, 2.08.

3.1.5.4 (3-(2-Chloroquinolin-3-yl)methylene)-5-(3-phenoxyphenyl)furan-2(3H)-one, 6a. Dark yellow, yield 78%, m.p. 216–218 °C, R_f 0.81, IR (cm^{-1}, ν_{max}, KBr) 1755 (C=O), 1623 (Aromatic C=C), 1215 (C–O), 1066 (ArC–N). ^{1}H NMR (CDCl$_3$, δ ppm) 6.89 (s, 1H, furanone ring), 7.34 (s, 1H, olefinic H), 7.89 (s, 1H, quinoline ring), 7.83 (s, 1H, quinoline ring), 6.97 (d, 1H, quinoline ring), 6.28 (d, 1H, quinoline ring), 6.47 (m, 1H, quinoline ring), 6.72 (s, 1H, ArH), 6.59 (s, 1H, ArH), 6.68 (s, 1H, ArH), 6.36 (s, 1H, ArH), 6.64 (d, 2H, ArH), 6.53 (d, 2H, ArH)and 6.13 (d, 1H,

ArH), ^{13}C NMR (100 MHz, CDCl$_3$) δ/ppm: 166.4 (1C, C-2), 137.2 (1C, C-3), 98.6 (1C, CH, C-4), 143.8 (1C, C-5), 139.6 (1C, CH, ethylene), 130.5 (1C, C-quinoline), 135.6 (1C, CH-quinoline), 126.4 (1C, C-quinoline), 128.4 (1C, CH-quinoline), 127.4 (1C, CH-quinoline), 130.8 (1C, -CH-quinoline), 127.5 (1C, CH-quinoline), 147.0 (1C, C-quinoline), 149.5 (1C, C-quinoline), 130.1 (1C, C-benzene), 119.5 (1C, CH-benzene), 128.2 (2C, CH-benzene), 116.7 (1C, CH-benzene), 159.9 (1C, C-benzene), 157.0 (1C, C-benzene), 117.5 (2C, CH-benzene), 128.6 (2C, CH-benzene), 121.9 (1C, CH-benzene) MS: m/z: 426 (M$^+$, 100%). Anal. calcd for C$_{26}$H$_{16}$ClNO$_3$: C, 73.33; H, 3.79; N, 3.38; found: C, 72.78; H, 4.19; N, 3.43.

3.1.5.5 (3-(2-Chloro-6-hydroxyquinolin-3-yl)methylene)-5-(3-phenoxyphenyl)furan-2(3H)-one, 6c. Light orange colour, yield 85%, m.p. 248–250 °C, Rf 0.87, IR (cm^{-1}, ν_{max}, KBr), 1760 (C=O), 1625 (Aromatic C=C), 1210 (C–O), 1063 (ArC–N). ^{1}H NMR (DMSO, δ ppm): 6.59 (s, 1H, furanone ring), 6.81 (s, 1H, olefinic H), 3.334 (broad s, 1H, OH), 9.125 (s, 1H, quinoline ring), 8.92 (s, 1H, quinoline ring), 8.00–8.02 (d, 1H, quinoline ring), 8.14–8.16 (d, 1H, quinoline ring), 7.36–7.40 (t, 3H, ArH), 7.84–7.87 (d, 2H, ArH), 7.40–7.47 (d, 2H, ArH), 7.53–7.58 (t, 2H, ArH), ^{13}C NMR (100 MHz, DMSO) δ/ppm: 142.6 (1C, C-benzene), 108.7 (2C, CH-benzene), 120.4 (2C, CH-benzene), 125.2 (1C, CH-benzene), 141.8 (1C, CH, ethylene), 134.9 (1C, C-quinoline), 130.6 (1C, CH-quinoline), 129.3 (1C, CH-quinoline), 108.9 (1C, CH-quinoline), 122.1 (1C, CH-quinoline), 130.8 (1C, -CH-quinoline), 147.4 (1C, C-quinoline), 156.2 (1C, C-quinoline), 142.5 (1C, CH-quinoline), 163.8 (1C, C-2), 133.8 (1C, C-3), 94.9 (1C, CH, C-4), 147.4 (1C, C-5), 132.3 (1C, C-benzene), 117.4 (1C, CH-benzene), 125.6 (1C, CH-benzene), 114.8 (1C, CH-benzene), 156.9 (2C, C-benzene), MS: m/z: 442 (M$^+$, 100%). Anal. calcd for C$_{26}$H$_{16}$ClNO$_4$: C, 70.67; H, 3.65; N, 3.17; found: C, 70.36; H, 3.49; N, 3.02.

3.1.5.6 (3-(2,6-Dichloroquinolin-3-yl)methylene)-5-(3-phenoxyphenyl)furan-2(3H)-one, 6e. Brown colour, yield 68%, m.p. 225–228 °C, R_f 0.82, IR (cm^{-1}, ν_{max}, KBr)1720 (C=O), 1628 (Aromatic C=C), 1225 (C–O), 1058 (ArC–N). ^{1}H NMR (CDCl$_3$, δ ppm): 6.86 (s, 1H, furanone ring), 7.59 (s, 1H, olefinic H), 7.81 (s, 1H, quinoline ring), 6.69 (s, 1H, quinoline ring), 6.62 (s, 1H, quinoline ring), 6.99 (s, 1H, quinoline ring), 6.73 (s, 1H, ArH), 6.54 (s, 1H, ArH), 6.98 (m, 2H, ArH), 6.74 (d, 1H, ArH), 7.22 (d, 2H, ArH), 6.92 (m, 1H, ArH) and 6.94 (d, 1H, ArH), ^{13}C NMR (100 MHz, CDCl$_3$) δ/ppm: 131.4 (1C, C-quinoline), 133.7 (1C, CH-quinoline), 126.5 (1C, CH-quinoline), 128.4 (1C, CH-quinoline), 132.2 (1C, CH-quinoline), 134.3 (1C, -CH-quinoline), 129.2 (1C, CH-quinoline), 145.6 (1C, C-quinoline), 148.6 (1C, CH-quinoline), 140.3 (1C, CH, ethylene), 165.5 (1C, C-2), 136.4 (1C, C-3), 99.8 (1C, CH, C-4), 145.9 (1C, C-5), 132.3 (1C, C-benzene), 118.2 (2C, CH-benzene), 126.3 (2C, CH-benzene), 125.2 (1C, CH-benzene), 152.8 (2C, C-benzene), 113.8 (1C, CH-benzene), 128.2 (1C, CH-benzene), 119.6 (1C, CH-benzene), 131.1 (1C, C-benzene), MS: m/z: 462 (M$^+$, 100%). Anal. calcd for C$_{26}$H$_{15}$Cl$_2$NO$_3$: C, 67.84; H, 3.28; N, 3.04; found: C, 65.98; H, 4.19; N, 3.11.

3.1.5.7 (3-(2-Chloro-6-fluoroquinolin-3-yl)methylene)-5-(3-phenoxyphenyl)furan-2(3H)-one, 6f. Yellow colour, yield 42%, m.p. 235–238 °C, R_f 0.83, IR (cm^{-1}, ν_{max}, KBr), 1722 (C=O), 1625 (Aromatic C=C), 1217 (C–O), 1025 (ArC–N). ^{1}H NMR (CDCl$_3$,

δ ppm): 6.82 (s, 1H, furanone ring), 7.64 (s, 1H, olefinic H), 7.92 (s, 1H, quinoline ring), 6.78 (s, 1H, quinoline ring), 6.53 (s, 1H, quinoline ring), 6.90 (s, 1H, quinoline ring), 6.72 (s, 1H, ArH), 6.47 (s, 1H, ArH), 6.53 (d, 2H, ArH), 6.77 (d, 1H, ArH), 7.19 (d, 2H, ArH), 6.95 (d, 1H, ArH) and 6.85 (d, 1H, ArH), ^{13}C NMR (100 MHz, CDCl$_3$) δ/ppm: 130.2 (1C, C-quinoline), 132.4 (1C, CH-quinoline), 127.3 (1C, CH-quinoline), 129.7 (1C, CH-quinoline), 130.9 (1C, CH-quinoline), 131.7 (1C, CH-quinoline), 126.1 (1C, CH-quinoline), 144.8 (1C, C-quinoline), 147.1 (1C, CH-quinoline), 141.5 (1C, CH, ethylene), 167.9 (1C, C-2), 138.9 (1C, C-3), 97.5 (1C, CH, C-4), 140.6 (1C, C-5), 134.6 (1C, C-benzene), 117.5 (2C, CH-benzene), 121.8 (2C, CH-benzene), 122.7 (1C, CH-benzene), 154.2 (2C, C-benzene), 115.7 (1C, CH-benzene), 124.3 (1C, CH-benzene), 118.2 (1C, CH-benzene), 133.4 (1C, C-benzene), MS: m/z: 446 (M$^+$, 100%). Anal. calcd for C$_{26}$H$_{15}$ClFNO$_3$: C, 68.83; H, 3.24; N, 3.06; found: C, 68.48; H, 3.29; N, 3.02.

3.1.5.8 (3-(2-Chloro-6-nitroquinolin-3-yl)methylene)-5-(3-phenoxyphenyl)furan-2(3H)-one, 6h. Yellowish orange crystals, yield 84%, m.p. 286–288 °C, R_f 0.84, IR (cm^{-1}, ν_{max}, KBr) 1765 (C=O), 1623 (Aromatic C=C), 1228 (C–O), 1065 (ArC–N). ^{1}H NMR (CDCl$_3$, δ ppm): 6.83 (s, 1H, furanone ring), 7.48 (s, 1H, olefinic H), 8.97 (s, 1H, quinoline ring), 8.46 (s, 1H, quinoline ring), 8.33 (s, 1H, quinoline ring), 8.24 (d, 1H, quinoline ring), 7.02 (d, 1H, ArH), 7.17 (s, 1H, ArH), 6.80 (s, 1H, ArH), 6.27 (s, 1H, ArH), 7.23 (d, 2H, ArH), 6.57 (m, 2H, ArH) and 6.97 (d, 1H, ArH), ^{13}C NMR (100 MHz, CDCl$_3$) δ/ppm: 166.3 (1C, C-2), 134.8 (1C, C-3), 96.4 (1C, CH, C-4), 146.1 (1C, C-5), 130.8 (1C, C-quinoline), 136.4 (1C, CH-quinoline), 124.8 (1C, CH-quinoline), 123.6 (1C, CH-quinoline), 147.3 (1C, CH-quinoline), 123.6 (1C, -CH-quinoline), 129.6 (1C, CH-quinoline), 148.4 (1C, C-quinoline), 152.9 (1C, CH-quinoline), 138.7 (1C, CH, ethylene), 131.3 (1C, C-benzene), 114.8 (2C, CH-benzene), 125.7 (2C, CH-benzene), 120.4 (1C, CH-benzene), 157.6 (1C, C-benzene), 156.9 (1C, C-benzene), 112.3 (1C, CH-benzene), 127.5 (1C, CH-benzene), 115.8 (1C, CH-benzene), 133.7 (1C, C-benzene), MS: m/z: 471 (M$^+$, 100%). Anal. calcd for C$_{26}$H$_{15}$ClN$_2$O$_5$: C, 66.32; H, 3.27; N, 5.78; found: C, 65.88; H, 3.20; N, 5.19.

3.1.5.9 5-(3-Benzylphenyl)-3-((2-chloroquinolin-3-yl)methylene)furan-2(3H)-one, 7a. Yield 73%; m.p. 110–112 °C, R_f 0.86, IR (KBr) cm^{-1} 1767 (C=O), 1563 (ArC=C), 1059 (ArC–N), 865 (ArC–H), 1215 (C–O), ^{1}H NMR (CDCl$_3$, δ ppm) 6.89 (s, 1H, furanone ring), 7.34 (s, 1H, olefinic H), 7.97 (s, 1H, quinoline ring), 7.88 (s, 1H, quinoline ring), 6.68 (d, 1H, quinoline ring), 6.61 (d, 1H, quinoline ring), 8.01 (m, 1H, quinoline ring), 3.82 (s, 2H, CH$_2$), 7.11 (m, 3H, ArH), 7.21 (d, 1H, ArH), 7.07 (t, 3H, ArH) and 7.06 (dd, 2H, ArH), ^{13}C NMR (100 MHz, CDCl$_3$) δ/ppm: 46.8 (1C, CH$_2$), 139.4 (1C, CH, ethylene), 141.9 (1C, C-benzene), 124.7 (2C, CH-benzene), 129.3 (2C, CH-benzene), 126.3 (1C, CH-benzene), 147.5 (1C, C-benzene), 136.4 (1C, C-benzene), 122.8 (1C, CH-benzene), 123.7 (1C, CH-benzene), 125.4 (1C, CH-benzene), 127.2 (1C, CH-benzene), 160.8 (1C, C-2), 138.2 (1C, C-3), 92.7 (1C, CH, C-4), 141.4 (1C, C-5), 138.1 (1C, C-quinoline), 140.2 (1C, CH-quinoline), 122.7 (1C, CH-quinoline), 121.9 (1C, CH-quinoline), 120.4 (1C, CH-quinoline), 123.2 (1C, -CH-quinoline), 130.4 (1C, CH-quinoline), 145.0 (1C, C-quinoline), 150.4 (1C, CH-quinoline), MS: m/z: 437 (M$^+$, 100%). Anal.

calcd for $C_{27}H_{18}ClNO_2$: C, 76.50; H, 4.28; N, 3.30; found: C, 75.48; H, 4.15; N, 3.49.

3.1.5.10 5-(3-Benzylphenyl)-3-((2-chloro-6-fluoroquinolin-3-yl) methylene)furan-2(3H)-one, 7f. Yield 76%; m.p. 150–152 °C, R_f 0.76, IR (KBr) cm^{-1} 1741 (C=O), 1558 (ArC=C), 1038 (ArC–N), 824 (ArC–H). ^{1}H NMR (CDCl$_3$): 6.91 (s, 1H, furanone ring),7.39 (s, 1H, olefinic proton), 7.81 (s, 1H, quinoline ring), 7.62 (s, 1H, quinoline ring), 7.58 (s, 1H, quinoline ring), 7.94 (s, 1H, quinoline ring), 7.16 (m, 5H, ArH), 3.69 (s, 2H, CH$_2$), 7.08 (d, 2H, ArH), 7.11 (s, 1H, ArH), 7.10 (s, 1H, ArH), ^{13}C NMR (100 MHz, CDCl$_3$) δ/ppm: 162.9 (1C, C-2), 142.7 (1C, C-3), 99.1 (1C, CH, C-4), 147.2 (1C, C-5), 38.3 (1C, CH$_2$), 135.8 (1C, CH, ethylene), 140.8 (2C, C-benzene), 128.1 (1C, CH-benzene), 119.6 (1C, CH-benzene), 117.4 (2C, CH-benzene), 124.9 (1C, CH-benzene), 132.3 (1C, C-benzene), 122.4 (1C, CH-benzene), 123.5 (1C, CH-benzene), 126.1 (1C, CH-benzene), 127.4 (1C, CH-benzene), 131.5 (1C, C-quinoline), 139.2 (1C, CH-quinoline), 127.1 (1C, CH-quinoline), 109.9 (1C, CH-quinoline), 161.1 (1C, C-quinoline), 120.8 (1C, -CH-quinoline), 129.3 (1C, CH-quinoline), 144.3 (1C, C-quinoline), 148.7 (1C, CH-quinoline), MS: m/z: 442 (M$^+$, 100%). Anal. calcd for $C_{27}H_{17}ClFNO_2$: C, 73.99; H, 3.88; N, 3.17; found: C, 72.78; H, 4.11; N, 3.28.

3.1.5.11 5-(3-Benzylphenyl)-3-((2-chloro-6-nitroquinolin-3-yl) methylene)furan-2(3H)-one, 7h. Yield 28%; m.p. 184–186 °C, R_f 0.71, IR (KBr) cm^{-1} 1767 (C=O), 1553 (ArC=C), 1051 (ArC–N), 838 (ArC–H), ^{1}H NMR (CDCl$_3$): 6.89 (s, 1H, furanone ring), 7.31 (s, 1H, olefinic proton), 8.23 (s, 1H, quinoline ring), 8.68 (s, 1H, quinoline ring), 8.46 (s, 1H, quinoline ring), 8.83 (s, 1H, quinoline ring), 2.84 (s, 2H, CH$_2$), 7.09 (m, 2H, ArH), 7.12 (s, 1H, ArH), 7.11 (s, 1H, ArH), 7.25 (m, 3H, ArH), 7.18 (m, 2H, ArH), ^{13}C NMR (100 MHz, CDCl$_3$) δ/ppm: 132.8 (1C, C-quinoline), 137.7 (1C, CH-quinoline), 126.9 (1C, CH-quinoline), 123.8 (1C, CH-quinoline), 146.7 (1C, C-quinoline), 124.2 (1C, -CH-quinoline), 128.1 (1C, CH-quinoline), 149.4 (1C, C-quinoline), 152.4 (1C, CH-quinoline), 167.3 (1C, C-2), 135.2 (1C, C-3), 91.4 (1C, CH, C-4), 144.1 (1C, C-5), 48.4 (1C, CH$_2$), 137.2 (1C, CH, ethylene), 141.6 (2C, C-benzene), 128.3 (2C, CH-benzene), 129.3 (2C, CH-benzene), 130.2 (2C, CH-benzene), 121.7 (1C, CH-benzene), 122.9 (1C, C-benzene), 120.1 (1C, CH-benzene), 113.8 (1C, CH-benzene), MS: m/z: 469 (M$^+$, 100%). Anal. calcd for $C_{27}H_{17}ClN_2O_4$: C, 69.19; H, 3.65; N, 5.97; found: C, 68.98; H, 3.53; N, 5.78.

3.2 *In vitro* test for antiplasmodial activity

3.2.1 Schizont maturation inhibition. The synthesized compounds were subjected to *in vitro* antiplasmodial activity (intraerythrocytic stage) against *Plasmodium falciparum* by Schizont Maturation Inhibition M-III method (WHO, 2001) with some modification. These compounds were solubilized in DMSO and the dilution was made with RPMI 1640 medium to adjust the concentration to 1 mg mL^{-1} before usage. The 96-well microtiter plates method was used in this procedure with dilution ranging between 1.56–100 μg mL^{-1}. 0.6–0.8% parasitemia were introduced in the culture and before the addition of drug solution, synchronization was done with 5–6% D-sorbitol. For tighter synchronization, it should be done several times until the ring-stage predominates in the cultures. Sorbitol destroys large

parasites (trophozoites and schizonts) in erythrocytes. Each well had 10 μL of parasite-infected erythrocytes, 5% hematocrit, and 90 μL of different drug dilutions. The concentration in the Standard drug and solvent control was the same as that of the test solution. The plates were incubated at 37 °C for one day. The blood sample from each well was taken, and a thin smear was produced on the cleaned glass slide. The Giemsa stain was used in the staining of the films. The optical-microscopy readings for the mature schizont count were done for each dilution and duplicate.

3.2.2 LDH inhibition assay. The final hematocrit in each sample from stoke solution, taken for the experiment was adjusted to 2% and parasitemia was made 0.5–1.0% by diluting with culture medium containing non-infected type O+ human erythrocytes. The compounds were solvated in the stock solution to get the concentration of 1 mg mL^{-1}. Subsequent dilutions were made with the culture medium containing 10% human serum. After that 10 μL of each stock solution at 5 different concentrations of two-fold dilutions were put into two 96-well microtiter plates in triplicate. Parasitized red blood cell suspensions (1–2% parasitemia) of 100 μL were then introduced to each well. Parasitized RBCs that lacked compounds were taken as control, while parasitized RBCs with chloroquine phosphate were used as standard wells. Incubation of plates was done in a CO$_2$ incubator. The plates were frozen at −20 °C for overnight after the incubation time, then defrosted to room temperature, and the process was repeated to haemolyse the RBC. The control cultures were considered for having 100% pLDH activity. After thawing, 5 μL of the supernatant suspension of blood was distributed into a microtitre plate which contained 25 μL Malstat reagent and 5 μL of 1/1 mixture of PES (phenazine ethosulfate, 2 mg mL^{-1}) and NBT (nitro blue tetrazolium, 0.1 mg mL^{-1}). The plates were then placed in the dark for **2h**, and absorption was measured at 650 nm. The calculation of IC values was done using Non-linear regression software. Individual dose–response curves and their corresponding IC values were determined.

3.3 Computational studies

3.3.1 Library generation of ligands. For the development of newer effective chemical entities, we planned to include quinoline moieties at α-position of the furanone ring so that some new compounds can be explored for anti-malarial potential. A series of a total of 24 hypothetical quinoline-furanone hybrids were designed based on the literature.

3.3.2 ADME-T prediction: the screening of the designed library of compounds. Schrodinger software QIKProp 3.6 and TOPKATmodule in Discovery Studio 2.5 were used. QIKProp requires Maestro-formatted maefiles (also referred to as 3D SD files) as input structures and gives information about several useful principal descriptors[27] such as molar weight (MW), lipophilicity parameter [log P(o/w)], number of rotatable bonds (NRB), number of hydrogen bond acceptors(HBA), number of hydrogen bond donors (HBD), total polar surface area (TPSA), solvent-accessible surface area (SASA), blood–brain partition coefficient (log BB), skin permeability (log Kp), solubility (log s), percentage human oral absorption, binding to human serum

albumin (log Khsa) apparent MDCK cell permeability (affyPMDCK), apparent Caco-2 cell permeability (affyPCaco) along with the Lipinski rule of 5.[28] A series of steps were performed for toxicity prediction in TOPKAT. The chemical structures were entered as the molfiles code and the relevant prediction module was selected. The specific chemical class sub-model is automatically chosen from the different chemical sub-models. TOPKAT informs the user whether the prediction is within the optimum prediction space (OPS) or not, reflecting the degree of confidence to assign to that prediction. The parameter OPS, enables the user to ascertain whether the test structure is contained in the model descriptor space. TOPKAT includes various toxicity modules, but carcinogenicity, and mutagenicity are considered the most important for preliminary toxicity prediction. In the current *in silico* studies of quinoline–furanone derivatives, toxicity predictions were made using the same module of carcinogenicity and mutagenicity.

3.3.3 Molecular docking studies. The possible target was recognized with the help of the BAITOC server provided by the Supercomputing Facility of Bioinformatics & Computational Biology (SCFBio), IIT Delhi, India. The protein *Plasmodium falciparum* lactate dehydrogenase (1LDG) was used in molecular docking studies to analyze the different binding poses of hypothesized ligands using the software MVD. The 3D structure of *Pf*LDH with co-crystallized NADH, and the substrate oxamate (1LDG) was downloaded from Protein Data Bank (https://www.rcsb.org). Finally, the 3D structure of the protein was imported into the workspace and prepared using a protein preparation wizard by removing the extra ligands and water molecules. The mol file of hypothetical ligands was also incorporated in the workspace and optimized by using the sequential steps given in ligprep. The steps like the interpretation of the missing charges, protonation states, and assigning the polar hydrogen to the protein; a cavity prediction algorithm to find the potential binding sites for ligands were done by the standard Molegro algorithm. The key amino acids of the binding pocket of the *Pf*LDH receptor were analyzed. After that various docking parameters were set such as the number of runs, number of poses, and conformations. At last docking wizard was run and moldock scores were noted down.

4. Conclusions

This studies revealed that all the synthesized hybrids showed antiplasmodial activity, but the compounds **5g** and **6e** showed maximum activity with IC_{50} value almost equal to the standard drug CQ and the compounds **5e, 5f, 6a, 6b, 7a** and **7f**, having IC_{50} value comparable to CQ(<5). However, two compounds **6c** and **7h** were exhibiting least antiplasmodial activity with IC_{50} >10.

The designed derivatives were made bulky to target the problem of drug efflux but at the same time, the compounds were exhibiting the drug like behavior with good ADME-T profile, confirmed by different *in silico* techniques. Moreover, binding mode analysis revealed that the ligands exhibited binding with the same active site residues, as reported for the cofactor NADH, which is reported essential for *Pf*LDH enzyme, therefore our designed compounds may have competition with

NADH for binding with enzyme. Moreover, similarity in binding mode with CQ which was reported as inhibitor of *Pf*LDH, revealed that these new hybrids can also act as *Pf*LDH inhibitors. Furthermore, the compounds with lower IC_{50} can be used as lead compounds for the designing and development of more potent and safe antiplasmodial agents as *Pf*LDH inhibitors.

Data availability

Data is contained within the article.

Conflicts of interest

The authors declare no conflict of interest.

Acknowledgements

References

1 World Health Organization, *WHO Guidelines for Malaria, 3 June 2022 (No. WHO/UCN/GMP/2022.01 Rev. 2)*, World Health Organization, 2019.

2 M. Loeffel and A. Ross, The relative impact of interventions on sympatric Plasmodium vivax and Plasmodium falciparum malaria: a systematic review, *PLoS Neglected Trop. Dis.*, 2022, **16**, 0010541, DOI: 10.1371/journal.pntd.0010541.

3 D. J. Kucharski, M. K. Jaszczak and P. J. Boratyński, A review of modifications of quinoline antimalarials: mefloquine and (hydroxy) chloroquine, *Molecules*, 2022, **27**, 1003, DOI: 10.3390/molecules27031003.

4 D. U. J. P. N'guessan, S. Coulibaly, A. E. M. Adouko and M. Ouattara, *Antimalarial Drugs with Quinoline Nucleus and Analogs*, 2023, DOI: 10.5772/intechopen.113193.

5 Y. Q. Hu, C. Gao, S. Zhang, L. Xu, Z. Xu, L. S. Feng and F. Zhao, Quinoline hybrids and their antiplasmodial and antimalarial activities, *Eur. J. Med. Chem.*, 2017, **139**, 22–47, DOI: 10.1016/j.ejmech.2017.07.061.

6 O. O. Ajani, K. T. Iyaye and O. T. Ademosun, Recent advances in chemistry and therapeutic potential of functionalized quinoline motifs–a review, *RSC Adv.*, 2022, **12**, 18594–18614, DOI: 10.1039/D2RA02896D.

7 L. S. Feng, Z. Xu, L. Chang, C. Li, X. F. Yan, C. Gao and X. Wu, Hybrid molecules with potential in vitro antiplasmodial and

in vivo antimalarial activity against drug-resistant Plasmodium falciparum, *Med. Res. Rev.*, 2020, **40**, 931–971, DOI: **10.1002/med.21643**.

8 J. A. Marinho, D. S. M. Guimarães, N. Glanzmann, G. de Almeida Pimentel, I. K. da Costa Nunes, H. M. G. Pereira and C. Abramo, In vitro and in vivo antiplasmodial activity of novel quinoline derivative compounds by molecular hybridization, *Eur. J. Med. Chem.*, 2021, **215**, 113271, DOI: **10.1016/j.ejmech.2021.113271**.

9 D. Choudhary, I. Rani, J. Monga, R. Goyal, A. Husain, P. Garg and S. L. Khokra, Pyrazole based furanone hybrids as novel antimalarial: A combined experimental, pharmacological and computational study, *Cent. Nerv. Syst. Agents Med. Chem.*, 2022, **22**, 39–56, DOI: **10.2174/1871524922666220301121811**.

10 M. Akhter, R. Saha, O. Tanwar, M. Mumtaz Alam and M. S. Zaman, Synthesis and antimalarial activity of quinoline-substituted furanone derivatives and their identification as selective falcipain-2 inhibitors, *Med. Chem. Res.*, 2015, **24**, 879–890, DOI: **10.1007/s00044-014-1139-1**.

11 R. Singh, V. Bhardwaj and R. Purohit, Identification of a novel binding mechanism of Quinoline based molecules with lactate dehydrogenase of Plasmodium falciparum, *J. Biomol. Struct. Dyn.*, 2021, **39**, 348–356, DOI: **10.1080/07391102.2020.1711809**.

12 D. Choudhary, G. K. Gupta and S. L. Khokra, Structure based designing and ADME-T studies of butenolide derivatives as potential agents against receptor ICAM-1: a drug target for cerebral malaria, *J. Comput. Sci.*, 2015, **10**, 156–165, DOI: **10.1016/j.jocs.2015.05.004**.

13 S. L Khokra, S. A Khan, D. Choudhary, S. M Hasan, A. Ahmad and A. Husain, Rational Design and Synthesis of Biologically Active Disubstituted 2 (3H) Furanones and Pyrrolone Derivatives as Potent and Safer NonSteroidal Anti-inflammatory Agents, *Anti-Inflammatory Anti-Allergy Agents Med. Chem.*, 2016, **15**, 54–71.

14 S. L. Khokra, P. Kaushik, M. M. Alam, M. S. Zaman, A. Ahmad, S. A. Khan and A. Husain, Quinoline based furanones and their nitrogen analogues: Docking, synthesis and biological evaluation, *Saudi Pharm. J.*, 2016, **24**, 705–717, DOI: **10.1016/j.jsps.2015.05.002**.

15 S. L. Khokra, S. A. Khan, P. Thakur, D. Chowdhary, A. Ahmad and A. Husain, Synthesis, molecular docking and potential antioxidant activity of di/trisubstituted pyridazinone derivatives, *J. Chin. Chem. Soc.*, 2016, **63**, 739–750, DOI: **10.1002/jccs.201600051**.

16 A. Husain, S. Khokra, P. Thakur, D. Choudhary, S. Kohli, A. Ahmad and S. Khan, Molecular modeling and in silico evaluation of novel pyridazinones derivatives as anticonvulsant agents, *In Silico Pharmacol.*, 2015, **1**, 7.

17 A. Husain, S. A. Khan, F. Iram, M. A. Iqbal and M. Asif, Insights into the chemistry and therapeutic potential of furanones: aa versatile pharmacophore, *Eur. J. Med. Chem.*, 2019, **171**, 66–92, DOI: **10.1016/j.ejmech.2019.03.021**.

18 F. Kayamba, T. Malimabe, I. K. Ademola, O. J. Pooe, N. D. Kushwaha, M. Mahlalela and R. Karpoormath, Design and synthesis of quinoline-pyrimidine inspired hybrids as potential plasmodial inhibitors, *Eur. J. Med. Chem.*, 2021, **217**, 113330, DOI: **10.1016/j.ejmech.2021.113330**.

19 L. F. Moor, T. R. Vasconcelos, R. da R Reis, L. S. Pinto and T. M. da Costa, Quinoline: an attractive scaffold in drug design, *Mini-Rev. Med. Chem.*, 2021, **21**, 2209–2226, DOI: **10.2174/1389557521666210210155908**.

20 R. Sharma, S. Patil and P. Maurya, Drug discovery studies on quinoline-based derivatives as potential antimalarial agents, *SAR QSAR Environ. Res.*, 2014, **25**, 189–203, DOI: **10.1080/1062936X.2013.875484**.

21 M. A. Salem, M. A. Gouda and G. G. El-Bana, Chemistry of 2-(piperazin-1-yl) quinoline-3-carbaldehydes, *Mini-Rev. Org. Chem.*, 2022, **19**, 480–495, DOI: **10.2174/1570193X18666211001124510**.

22 P. Sharma, C. R. Pillai and J. D. Sharma, In vitro schizontocidal activity of standard antimalarial drugs on chloroquine-sensitive and chloroquine-resistant isolates of Plasmodium falciparum, *Indian J. Exp. Biol.*, 2000, **38**, 1129–1133.

23 S. M. Smith, M. B. Wunder, D. A. Norris and Y. G. Shellman, A simple protocol for using a LDH-based cytotoxicity assay to assess the effects of death and growth inhibition at the same time, *PLoS One*, 2011, **6**, e26908, DOI: **10.1371/journal.pone.0026908**.

24 S. S. Muttaqin and J. S. Maji, Screening of oxamic acid similar 3D structures as candidate inhibitor Plasmodium falciparum L-lactate dehydrogenase of malaria through molecular docking, in *2018 1st International Conference on Bioinformatics, Biotechnology, and Biomedical Engineering-Bioinformatics and Biomedical Engineering*, 2018, vol. 1, pp. 1–6, DOI: **10.1109/BIOMIC.2018.8610537**.

25 B. Chandrasekaran, S. N. Abed, O. Al-Attraqchi, K. Kuche and R. K. Tekade, Computer-aided prediction of pharmacokinetic (ADMET) properties, in *Dosage Form Design Parameters*, Academic Press, 2018, pp. 731–755, DOI: **10.1016/B978-0-12-814421-3.00021-X**.

26 I. A. Shehadi, H. R. Rashdan and A. H. Abdelmonsef, Homology modeling and virtual screening studies of antigen MLAA-42 protein: identification of novel drug candidates against leukemia—an in silico approach, *Comput. Math. Methods Med.*, 2020, **2022**(1), 1–12, DOI: **10.1155/2020/8196147**.

27 Z. Y. U. Ibrahim, A. Uzairu, G. Shallangwa and S. Abechi, Molecular docking studies, drug-likeness and in-silico ADMET prediction of some novel β-Amino alcohol grafted 1, 4, 5-trisubstituted 1, 2, 3-triazoles derivatives as elevators of p53 protein levels, *Sci. Afr.*, 2020, **10**, e00570, DOI: **10.1016/j.sciaf.2020.e00570**.

28 M. Sinha, A. Dhawan and R. Parthasarathi, In silico approaches in predictive genetic toxicology, *Methods Protoc.*, 2019, 351–373.